Large-scale structural changes in the sarcoplasmic reticulum ATPase appear essential for calcium transport

J. K. Blasie, D. Pascolini, F. Asturias, L. G. Herbette, D. Pierce, and A. Scarpa
Department of Chemistry, University of Pennsylvania, Philadelphia, Pennsylvania 19104 USA

ABSTRACT Model refinement calculations utilizing the results from time-resolved x-ray diffraction studies indicate that specific, large-scale changes (i.e., structural changes over a large length scale or long range) occur throughout the cylindrically averaged profile structure of the sarcoplasmic reticulum ATPase upon its phosphorylation during calcium active transport. Several physical-chemical factors, all of which slow the kinetics of phosphoenzyme formation, induce specific, large-scale changes throughout the profile structure of the unphosphorylated enzyme that in general are opposite to those observed upon phosphorylation. These results suggest that such large-scale structural changes in the ATPase occurring upon its phosphorylation are required for its calcium transport function.

INTRODUCTION

The active (energy-dependent) transport of calcium from the cytoplasm across the sarcoplasmic reticulum membrane into the sarcotubular system by the membrane Ca^{2+} ATPase is responsible for the relaxation phase of the contraction-relaxation cycle in striated and cardiac muscle (1). Since the sarcoplasmic reticulum membrane can be isolated in the form of closed unilamellar vesicles in which the Ca^{2+} ATPase comprises over 90% of the membrane protein (2), the enzyme-catalyzed reactions involved in the calcium active transport process (3), and the structure and organization of the membrane components (4) have been relatively well characterized. As a result, this system provides an excellent prototype for the study of critical structure-function relationships involved in the active transport of ions across biological membranes.

In the course of our structural and functional studies of the Ca^{2+} ATPase of the sarcoplasmic reticulum (SR), we have previously determined the separate profile structures of the phospholipid bilayer and the Ca^{2+} ATPase protein within fully functional, isolated sarcoplasmic reticulum membranes (5, 6). Those structural studies utilized meridional x-ray and neutron diffraction from oriented membrane multilayers coupled with the perdeuteration of the membrane phospholipids and H_2O/D_2O exchange and provided the profile structure of the ATPase to ~12 Å resolution, as cylindrically averaged about the membrane normal by the smectic liquid-crystalline order in the membrane. We have also analyzed the multiphasic kinetics of calcium active transport by these isolated SR membranes in the form of unilamellar vesicular dispersions as compared with oriented membrane multilayers. That work employed the flash-photolysis of caged ATP and double-beam spectrophotometry of metallochromic dyes localized in the extravesicular medium to initiate and monitor the calcium active transport by the ATPase ensemble (7, 8). A fast phase of calcium uptake was associated with the formation of the first phosphorylated enzyme intermediate $E_1 \sim P$ and the "occlusion" of the two high-affinity calcium-binding sites.[1] This was followed by a slow phase of calcium uptake associated with the translocation of calcium across the membrane profile, as identified by its sensitivity to ionophores rendering the membrane permeable to calcium.[1]

Using the above-mentioned work as an essential basis, we then performed time-resolved x-ray diffraction studies to investigate whether large-scale changes (i.e., large length-scale or long-range structural changes) in the moderate resolution Ca^{2+} ATPase profile structure were associated with the ATP-induced calcium transport process (9, 10). Those studies employed focused, monochro-

D. Pascolini's present address is The Wistar Institute, Philadelphia, PA 19104.

L. G. Herbette's present address is Departments of Radiology, Medicine and Biochemistry, University of Connecticut Health Center, Farmington, CT 06032.

A. Scarpa's present address is Department of Physiology and Biophysics, Case Western Reserve University, Cleveland, OH 44106.

[1]Two Ca^{2+} ions per protein molecule are bound to all forms of the ATPase enzyme referred to in this paper. To simplify the notation, the Ca^{2+} ions have been omitted. The first phosphorylated intermediate, for example, is denoted as $E_1 \sim P$ instead of $(Ca^{2+})_2E_1 \sim P$.

0006-3495/90/09/687/07 $2.00

matic synchrotron x-radiation from both bending-magnet and wiggler-magnet beam-lines at the Stanford Synchrotron Radiation Laboratory. The calcium active transport process was synchronously (on the millisecond timescale) initiated among the ATPase ensemble in the oriented membrane multilayer by the flash photolysis of caged ATP. A SIT image-intensifier-based detector was used to record the meridional diffraction data in 0.2–5.0 s time-frames. Because the temperature-dependent lifetimes of the more interesting first and second phosphorylated intermediate forms of the enzyme, $E_1 \sim P$ and $E_2 \sim P$ vary from a few hundred milliseconds to a few seconds (11) over the temperature range for which the membrane multilayers are stable ($-2° \leq T \leq 15°C$), the inherently slow read-out time of the detector pixel array (many seconds) prevented "time-slicing," (i.e., the recording of sequential time-frames of 0.2–5.0 s duration with only negligible delay between frames). Therefore, we focussed our attention on the comparison of the "resting" E_1 vs. the $E_1 \sim P$ forms of the enzyme. The highly reproducible (multilayer to multilayer; see reference 10 for details) and reversible (for each multilayer) changes in the profile structure of the SR membrane upon $E_1 \sim P$ formation in the oriented membrane multilayer at -2–$0°C$, utilizing 2–5-s timeframes, are shown in Fig. 1 (taken from reference 10). These changes are very similar to those observed at 6–8°C, utilizing 0.2–0.5-s timeframes. No such changes in the membrane profile structure were observable upon the flash photolysis of caged ADP under otherwise identical conditions in the multilayer, thereby providing a critical control against artifacts arising from the flash-photolysis reactions. A qualitative interpretation of these changes in the SR membrane profile structure upon $E_1 \sim P$ formation indicated a large-scale (or long-range) redistribution of protein mass from the ATPase "headpiece" (which protrudes from the extravesicular surface of the membrane lipid bilayer) into the lipid hydrocarbon core region of the membrane profile, namely a *net inward* movement of the ATPase mass into the nonpolar core of the membrane.

While the above-mentioned time-resolved structural studies clearly identified the specific changes in the SR membrane profile structure associated with the ATP-induced formation of $E_1 \sim P$ from E_1, they alone could not address the significance of these changes to the actual calcium active-transport process. It was suggested from the literature that manipulation of several physical-chemical parameters available to this membrane multilayer system might be utilized to slow the ATP-induced formation, and/or extend the lifetime (i.e., "transient trapping") of $E_1 \sim P$, the latter also slowing the formation of $E_2 \sim P$ from $E_1 \sim P$ *without totally inhibiting* enzyme turnover. Upon further investigation of the ATP-induced calcium transport kinetics, we verified that low temperature (relative to the upper characteristic temperature t_h for lipid lateral phase separation, see below), "low" [Mg^{2+}] (micromolar vs. millimolar), and relatively low water content (in the partially dehydrated, oriented multilayers vs. vesicular dispersions), all slowed the

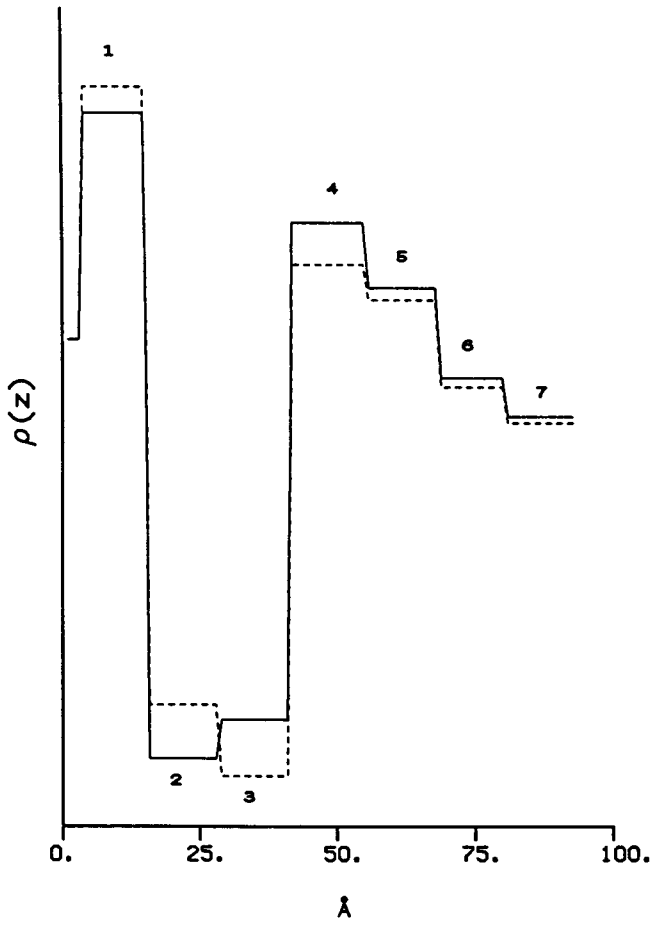

FIGURE 1 Step-function model profiles at moderate resolution (17 Å) for a single SR membrane profile (the multilayer unit cell profile contains two apposed single membranes each within $0 \leq z \leq 106$ Å): the solid line is the step-function model profile for the SR membrane immediately before the UV flash-photolysis of caged ATP, the dashed line for the SR membrane immediately after the UV flash. The profiles were derived from the analysis of the time-resolved x-ray diffraction experiments performed at 0 to $-$ 2°C and with a time resolution of 2–5 s. The numbers identify the following regions of the membrane profile: 1 and 4, the lipid polar headgroup region of the inner and outer monolayer, respectively; 2 and 3, the lipid fatty acyl chain region of the inner and outer monolayer, respectively; 5–7 the extravesicular surface of the membrane (outside the lipid bilayer) containing the ATPase "headpiece"; the region about $z = 0$ corresponds to the intravesicular water space. The changes in the SR membrane step-function model profile upon the UV flash photolysis of caged ATP under these conditions arise from $E_1^+ \sim P$ formation from E_1^+, and include a decrease of density for steps 3 and 4 and a corresponding gain of density for steps 1 and 2; only a small change (decrease) of density occurs for steps 5–7. For the interpretation of these changes see the text and Figs. 3 and 4.

formation of $E_1 \sim P$ and extended its lifetime to varying degrees, thereby only slowing overall enzyme turnover without rendering the enzyme nonfunctional (12). Upon subsequent investigation of the SR membrane profile structure for the "resting" E_1 form of the ATPase as a function of the three thermodynamic variables temperature, $[Mg^{2+}]$ and $[H_2O]$ in the oriented multilayers, we discovered a well-defined transition temperature for a large-scale (or long-range) structural change in the membrane profile, closely associated with the onset of lipid lateral-phase separation (the formation of two-dimensionally crystalline domains of frozen lipid chains in the membrane plane) in the membrane (12, 13). The transition temperature for the membrane profile structure invariably occurred near the upper characteristic temperature t_h for the onset of lipid lateral-phase separation, which varies significantly as a function of the two other parameters ($[Mg^{2+}]$ and $[H_2O]$) studied. Upon lowering the temperature through the transition, the membrane profile structure for the "resting" E_1 form of the ATPase changes to that corresponding to a different moderate-resolution conformation for the ATPase, which we denote as E_1^+, as shown in Fig. 2. A qualitative interpretation of these changes indicated a large-scale (or long-range) redistribution of the ATPase mass *outward* from the lipid hydrocarbon core region of the membrane profile into the "headpiece" region. Qualitatively similar structural changes in the membrane profile are observed upon lowering the temperature through the transition temperature, as it varies with $[Mg^{2+}]$ and $[H_2O]$ in the multilayer. Comparison of the $[Mg^{2+}]$ and $[H_2O]$ dependence of the structural transition temperature with the results from the corresponding ATP-induced calcium transport kinetics studies strongly indicates that it is this structural transition in the membrane profile which is responsible for the slowing of $E_1 \sim P$ formation and its "transient trapping." For example, at high $[Mg^{2+}]$ (~25 mM) and relatively low $[H_2O]$ the transition in the membrane profile structure occurs at 2–3°C, which corresponds to the temperature below which a considerable extension of $E_1 \sim P$ lifetime is observed.

In this paper, we present model refinement calculations that allow a more quantitative description of the changes in the profile structure of the ATPase at moderate resolution required to account for the changes in the SR membrane profile associated with the $E_1 \rightarrow E_1 \sim P$, $E_1^+ \sim P$, and $E_1 \rightarrow E_1^+$ transitions in the form of the enzyme.

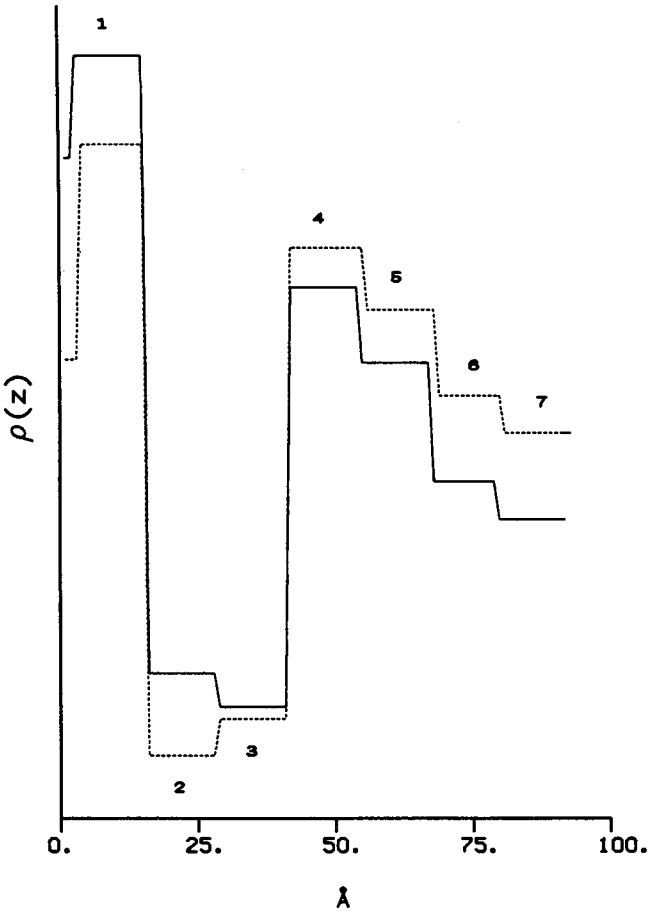

FIGURE 2 Step-function model profiles at 16–17 Å resolution for a single SR membrane profile in an oriented multilayer at high $[Mg^{2+}]$ (~25 mM) as a function of temperature. The numbers (1–7) identify the steps with the regions of a single SR membrane profile, as in Fig. 1. The solid line is the step-function model profile for an SR membrane multilayer in full equilibrium at 7.5°C, i.e., above the transition temperature (2–3°C). Partial dehydration of the multilayers at temperatures below the transition temperature, e.g. −2–0°C, results in their full equilibration at that temperature and the step-function model profile shown by the dotted line. The changes in the SR membrane profile upon lowering the temperature through the transition temperature resulting in the transition from E_1 to the E_1^+ form of the ATPase include a decrease of density for steps 1–3 and for the region about $z = 0$, i.e., the intravesicular water space, and an increase of density for steps 4–6. For the interpretation of these changes, see the text and Figs. 3 and 4.

METHODS

The SR membrane profiles shown in Figs. 1 and 2 (as step-function, relative electron density profiles) were subjected to model refinement calculations analogous to those performed previously on this and other membrane systems (4–6, 9, 14–16), to provide the fraction of the area occupied in the membrane plane by each of the membrane's molecular components within each of the different distinguishable regions of the membrane profile (as determined by the spatial resolution of the profile). Area profiles for the SR membrane components for the E_1 form of the ATPase were calculated to conform with the phospholipid asymmetry between the inner and outer monolayers of the membrane lipid bilayer and the protein profile, as experimentally determined previously via neutron diffraction (5). This refinement calculation employed the following simplified expression for the electron density profile for a

three-component membrane:

$$\rho_m(k) = \bar{\rho}_p \cdot A_p(k) + \bar{\rho}_l(k) \cdot A_l(k) + \bar{\rho}_w \cdot A_w(k), \quad (1)$$

where $k = 1 \rightarrow 7$ is the index of the seven resolution-limited steps in the profiles of Figs. 1 and 2, $\bar{\rho}_p$ is the average electron density of the protein component, $A_p(k)$ is the fractional area in the membrane plane occupied by the protein component in the kth step, $\bar{\rho}_l(k)$ is the average electron density of the phospholipid component in the kth step, allowing for the average electron density difference for the headgroups vs. the hydrocarbon chains, $A_l(k)$ is the fractional area in the membrane plane occupied by the phospholipid component in the kth step, and similarly for the water component via $\bar{\rho}_w$ and $A_w(k)$. Furthermore, the constraint $[A_p(k) + A_l(k) + A_w(k)] = A_{tot}$ for all k was utilized. The area profiles for the SR membrane components for the E_1^+ and $E_1^+ \sim P$ forms of the ATPase were then calculated, assuming that the respective temperature induced ($E_1 \rightarrow E_1^+$) and phosphorylation induced ($E_1^+ \rightarrow E_1^+ \sim P$) changes in the corresponding membrane profiles were dominated by changes in the fractional areas occupied by the three components, namely $A_p(k)$, $A_l(k)$, and $A_w(k)$, while maintaining the constraint $[A_p(k) + A_l(k) + A_w(k)] = A_{tot}$ for all k-steps *and* the constants $\bar{\rho}_p$, $\bar{\rho}_l(k)$, and $\bar{\rho}_w$; as such, these model refinement calculations provide the *maximal* changes (see Discussion) in the ATPase area profile associated with $E_1 \rightarrow E_1^+$ and $E_1^+ \rightarrow E_1^+ \sim P$ transitions in the form of the enzyme.

This approach therefore models these changes in the three-component membrane profile according to the expression:

$$\Delta\rho_m(k) = \bar{\rho}_p \cdot \Delta A_p(k) + \bar{\rho}_l(k) \cdot \Delta A_l(k) + \bar{\rho}_w \cdot \Delta A_w(k), \quad (2)$$

which is a considerable simplification of the correct general expression,

$$\Delta\rho_m(k) = \Delta[\bar{\rho}_p(k) \cdot A_p(k) + \bar{\rho}_l(k) \cdot A_l(k) + \bar{\rho}_w(k) \cdot A_w(k)], \quad (3)$$

for even such a simple three-component membrane. An alternate simplification of the general expression provides:

$$\Delta\rho_m(k) = A_p(k) \cdot \Delta\bar{\rho}_p(k) + A_l(k) \cdot \Delta\bar{\rho}_l(k) + A_w(k) \cdot \Delta\bar{\rho}_w(k), \quad (4)$$

whereby the changes in the membrane profiles would be assumed to be dominated by changes in the apparent electron densities of the three components, while maintaining constant their respective areas occupied in the membrane plane $A_p(k)$, $A_l(k)$, and $A_w(k)$. The results of the model refinement calculations must necessarily reflect any simplifying assumptions made. We have chosen to utilize the simplification of expression 2 because of insufficient experimental evidence to establish reasonable constraints on the allowable $\Delta\rho_p$, etc. required for utilization of the alternate simplification of expression 4. However, we will demonstrate in the Discussion that our overall conclusions are indeed similar, utilizing either of the simplifications of expressions 2 or 4. Needless to say, the correct general expression 3 for $\Delta\rho_m(k)$ is even less constrained in the absence of additional information, for example, as provided from neutron diffraction.

RESULTS

The area profiles at moderate resolution (~17 Å) for the separate Ca^{2+} ATPase protein, phospholipid and water components for a single SR membrane are shown in Fig. 3

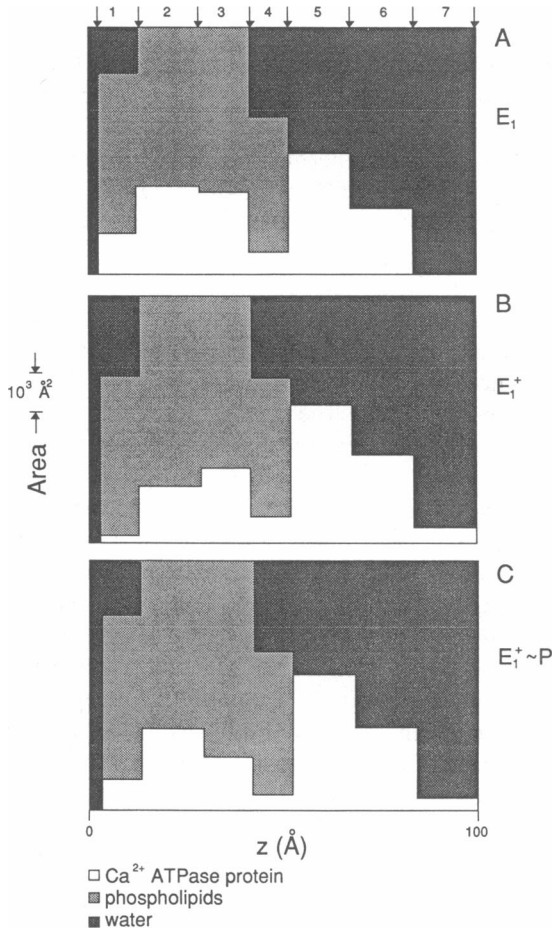

FIGURE 3 Area profiles at moderate resolution (~17 Å) for the separate Ca^{2+} ATPase protein, phospholipid, and water components for a single SR membrane. These area profiles are derived from the membrane electron density profiles (10, 13) and represent the area occupied in the membrane plane by each of the membrane's molecular components within each of the different resolution-limited regions of the membrane profile. (*A*) Area profiles for the SR membrane components at rest at 6–8°C, i.e., for the E_1 form of the ATPase; they are consistent with the phospholipid asymmetry between inner versus outer monolayers of the membrane lipid bilayer, and with the protein profile determined previously (5). Upon lowering the temperature through the structural transition temperature for the resting state of the Ca^{2+} ATPase, the area profile for the protein changes to the one shown in *B*, characterizing the E_1^+ form of the ATPase. Upon enzyme phosphorylation and formation of $E_1^+ \sim P$ from E_1^+, the protein area profile changes to that shown in *C*. The area profiles in *A–C* are totally consistent with the step-function model profiles in Figs. 1 and 2; the arrows delimit the seven regions in the area profiles corresponding to the regions with the same number in the step-function model profiles of Figs. 1 and 2. The area profiles shown in *B* and *C* were calculated assuming that the respective temperature-induced and phosphorylation-induced changes in the membrane profile were dominated by changes in the area profiles of the three membrane components, while maintaining the constraint $[A_p(k) + A_l(k) + A_w(k)] = A_{tot}$ for all steps indexed $k = 1 \rightarrow 7$ and the constants $\bar{\rho}_p$, $\bar{\rho}_l(k)$ and $\bar{\rho}_w$ (see test and references 10, 12, 13).

for the E_1, E_1^+, and $E_1^+ \sim P$ forms of the enzyme. Upon lowering the temperature through the structural transition for the resting E_1 form of the ATPase, the area profile for the protein changes from that of Fig. 3 *A* for the E_1 form to that of Fig. 3 *B* for the E_1^+ form of the enzyme; this structural change in the ATPase protein profile consists of a large-scale or long-range (mass-conserving) redistribution of as much as 15% of the total ATPase mass *outward* from the lipid hydrocarbon core region of the membrane profile into the "headpiece" region. Upon phosphorylation of the E_1^+ form of the enzyme, the area profile for the protein changes from that of Fig. 3 *B* for the E_1^+ form to that of Fig. 3 *C* for the $E_1^+ \sim P$ form of the enzyme; this structural change in the ATPase protein profile consists of a large-scale or long-range (mass conserving) redistribution of as much as 10% of the total ATPase mass *inward* from the "headpiece" region into the lipid hydrocarbon core region of the membrane profile. Similar changes occur in the ATPase protein profile for the $E_1 \rightarrow E_1 \sim P$ transition (not shown, see reference 9).

DISCUSSION

On the basis of these model refinement calculations and the prior work from this laboratory briefly described in the Introduction, it has been reasonably established that very similar large-scale (or long-range) structural changes occur throughout the SR membrane Ca^{2+} ATPase profile upon the ATP-induced formation of $E_1 \sim P$ from E_1, and the slower formation of $E_1^+ \sim P$ from E_1^+. These changes that occur upon phosphorylation of the ATPase enzyme comprise a net *inward* movement of protein mass from the ATPase "headpiece" on the extravesicular surface into the lipid hydrocarbon core region of the membrane profile; such changes are shown pictorially in Fig. 4 *C*. Conversely, it has been similarly demonstrated that large-scale (or long-range) structural changes in the "resting" E_1 form the ATPase which result in the E_1^+ form are responsible for slowing the kinetics of its ATP-induced phosphorylation to $E_1^+ \sim P$. These structural changes generally comprise a net *outward* movement of protein mass from the lipid hydrocarbon core to the ATPase "headpiece" on the extravesicular surface region of the membrane profile, and are shown pictorially in Fig. 4 *B*. Therefore, the structural changes in the "resting" E_1 form of the ATPase induced via manipulation of parameters of the membrane phase diagram that result in the E_1^+ form and in the slowing of ATP-induced $E_1^+ \sim P$ formation are basically *opposite* to those structural changes that occur upon ATP-induced phosphorylation of either E_1 or E_1^+. The structural changes in the

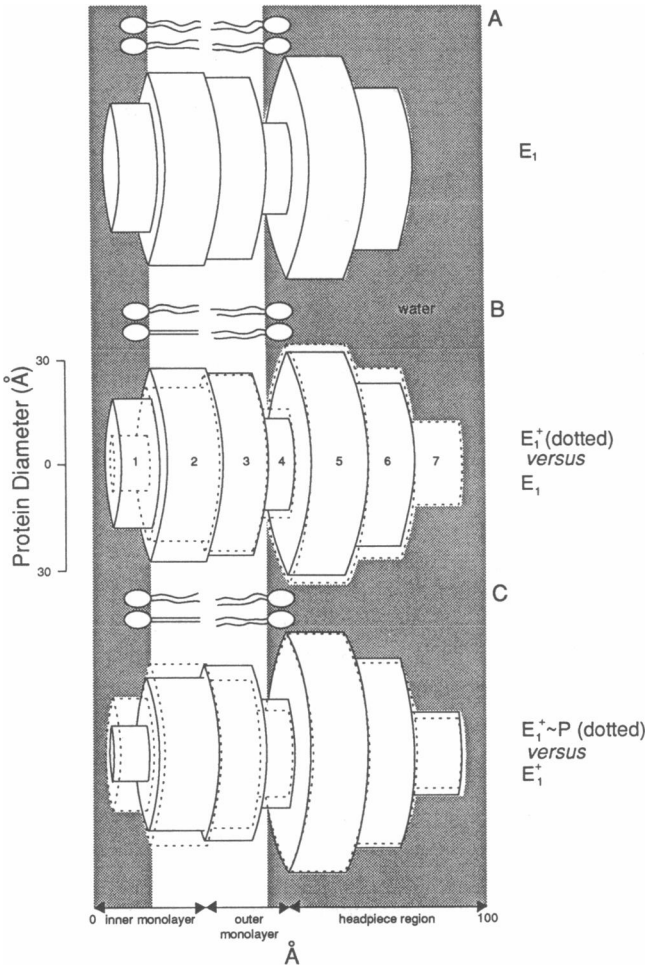

FIGURE 4 Pictorial representation of the cylindrically averaged (about the normal to the membrane plane) Ca^{2+} ATPase protein structure based on the area profiles shown in Fig. 3. (*A*) The resting state E_1 at 6–8°. (*B*) In the resting state E_1^+ at 0 to −2°C. (*C*) The transiently trapped phosphorylated intermediate state $E_1^+ \sim P$ at 0 to −2°C. In *B*, the dotted-line cylinder represents the E_1^+ form of the protein, whereas in *C*, the dotted-line cylinder represents the $E_1^+ \sim P$ form of the protein. The numbers 1–7 in *B* correlate the cylindrical regions representing the protein with the regions in the step-function model profiles of Figs. 1 and 2. This representation also assumes that the respective phosphorylation-induced and temperature-induced changes in the membrane profile are dominated by changes in the area profiles of the three membrane components, while maintaining the constraint $[A_p(k) + A_l(k) + A_w(k)] = A_{tot}$ for all steps indexed $k = 1 \rightarrow 7$ and the constants $\bar{\rho}_p$, $\bar{\rho}_l(k)$ and $\bar{\rho}_w$ (see text and references 10, 12, 13).

"resting" E_1 form of the SR ATPase responsible for slower phosphorylation produce an ATPase structure, E_1^+, and the structural differences between E_1^+ and the corresponding phosphorylated intermediate $E_1^+ \sim P$ are larger than the differences between the E_1 and $E_1 \sim P$ forms, especially within the more conformationally restric-

tive lipid bilayer region of the membrane. Hence, the overall activation energy barrier in the ATPase polypeptide's configurational free-energy surface is significantly greater for the formation $E_1^+ \sim P$ from E_1^+, as compared with that for the formation of $E_1 \sim P$ from E_1. The fact that changes in the structure of the protein that slow active calcium transport are opposite to those that occur upon enzyme phosphorylation strongly suggests that the large-scale or long-range structural changes observed upon phosphorylation of the enzyme are essential for its active calcium transport function.

With regard to the above discussion, the following points should be noted: (*a*) The changes in the SR membrane profile associated with the transitions $E_1 \leftrightarrow E_1^+$, $E_1 \leftrightarrow E_1 \sim P$ and $E_1^+ \leftrightarrow E_1^+ \sim P$ of the ATPase are rapid and reversible. The timescales for these transitions are all sufficiently short that we did not consider phospholipid "flip-flop" as a possible contributor to the observed changes in the SR membrane profile (9, 10, 12, 13).

(*b*) The changes in the SR membrane profile associated with these transitions of the ATPase could also conceivably arise from order-disorder transitions in the ATPase and/or phospholipid components of the membrane, which would be more consistent with the alternate simplification (expression 4) for $\Delta\rho_m(k)$, assuming the changes in the membrane profiles to be dominated by changes in the apparent electron densities of the membrane components, while maintaining their respective areas in the membrane plane constant (see Methods). Assuming that the changes in the SR membrane profile described arise exclusively from such order-disorder transitions, then the $E_1 \rightarrow E_1 \sim P$ and $E_1^+ \rightarrow E_1^+ \sim P$ transitions in the ATPase would require a disordering of the ATPase "headpiece" and of the ATPase and/or phospholipid within the outer monolayer of the membrane lipid bilayer, and an ordering of the ATPase and/or phospholipid within the inner monolayer upon enzyme phosphorylation. Conversely, the temperature-induced $E_1 \rightarrow E_1^+$ transition in the ATPase would require an ordering of the ATPase "headpiece" and of the ATPase and/or phospholipid in the outer monolayer and a disordering of the ATPase and/or phospholipid in the inner-monolayer of the membrane lipid bilayer. Thus, even in this other extreme of interpretation, the structural changes (in terms of exclusively order-disorder transitions) must involve the ATPase, are large-scale or long-range, spanning the entire membrane profile, and are opposite in nature for the $E_1 \rightarrow E_1 \sim P$ and $E_1^+ \rightarrow E_1^+ \sim P$ versus the $E_1 \rightarrow E_1^+$ transitions of the ATPase. As a result, the overall conclusions of this work remain, namely that large-scale or long-range changes in the SR membrane profile occur upon enzyme phosphorylation *and* that they appear essential for active calcium transport.

(*c*) Our assumption that the phosphorylation-induced and temperature-induced changes in the SR membrane profile were dominated by changes in the area profiles of the three membrane components, while maintaining the total area constraint $[A_p(k) + A_l(k) + A_w(k)] = A_{tot}$, and the constants $\bar{\rho}_p$, $\bar{\rho}_l(k)$, and $\bar{\rho}_w$, results in a maximization of the protein mass redistributions required to explain the changes in the membrane profile. In terms of (*b*) above, we provide one example to illustrate the point: From Fig. 3, *B* and *C*, the transition from $E_1^+ \rightarrow E_1^+ \sim P$ results in an increase in ATPase mass in the hydrocarbon core of the inner lipid monolayer (region "2" of the area profiles), i.e., increased $A_p(2)$ at constant $\bar{\rho}_p$. In the absence of phospholipid "flip-flop" on the phosphorylation timescale, the fatty-acid chains of the inner monolayer must therefore occupy less area $A_l(2)$ in the membrane plane, namely by ordering and thereby raising their density $\bar{\rho}_l(2)$. Hence, both ATPase protein mass increase and the resulting phospholipid hydrocarbon chain ordering contribute to the increased electron density of region "2" in Fig. 1, upon enzyme phosphorylation. As a result of our assumptions (namely, constant $\bar{\rho}_p(2)$ and $\bar{\rho}_l(2)$ in this case), the contribution of ATPase mass increase to region "2" upon enzyme phosphorylation has been overestimated. Similar arguments can apply to the other regions of the membrane profile containing the lipid bilayer (regions "1–4") and also the ATPase "headpiece" (regions "5–7"), where water solvates the ATPase instead of phospholipid.

CONCLUSION

We have presented evidence that large-scale or long-range structural changes occur over the SR membrane profile upon enzyme phosphorylation during active calcium transport, and that these large-scale or long-range changes appear essential for the active calcium transport function. These large-scale structure changes have been quantitatively accounted for in a manner which necessarily maximized the contribution of ATPase mass redistribution across the SR membrane profile. Phosphorylation-induced ordering/disordering of the ATPase polypeptide, and the resulting ordering/disordering of the phospholipid/water solvating the protein in the different regions of the membrane profile may also contribute to these essential structural changes in the SR membrane profile.

REFERENCES

1. Ebashi, S., M. Endo, and I. Ohtsuki. 1969. Control of muscle contraction. *Q. Rev. Biophys.* 2:351–384.

2. Meissner, G., G. E. Conner, and S. Fleischer. 1973. Isolation of sarcoplasmic reticulum by zonal centrifugation and purification of Ca^{2+}-pump and Ca^{2+}-binding proteins. *Biochim. Biophys. Acta.* 298:246–269.

3. DeMeis, L., and A. L. Vianna. 1979. Energy interconversion by the Ca^{2+}-dependent ATPase of the sarcoplasmic reticulum. *Annu. Rev. Biochem.* 48:275–292.

4. Blasie, J. K., L. Herbette, and J. M. Pachence. 1985. Biological membrane structure as "seen" by x-ray and neutron diffraction. *J. Membr. Biol.* 86:1–7.

5. Herbette, L., P. DeFoor, S. Fleischer, D. Pascolini, A. Scarpa, and J. K. Blasie. 1985. The separate profile structures of the calcium pump protein and the phospholipid bilayer within isolated sarcoplasmic reticulum membrane determined by x-ray and neutron diffraction. *Biochim. Biophys. Acta.* 817:103–122.

6. Blasie, J. K., J. M. Pachence, and L. Herbette. 1983. Comment on the importance of appropriate neutron diffraction data in the decomposition of membrane scattering profiles into the separate scattering profile of their molecular components. *Neutrons Biol.* 27:201–210.

7. Pierce, D., A. Scarpa, M. R. Topp, and J. K. Blasie. 1983. Kinetics of calcium uptake by the sarcoplasmic reticulum vesicles using flash photolysis of caged adenosine 5′-triphosphate. *Biochemistry.* 22:5254–5261.

8. Pierce, D., A. Scarpa, D. R. Trentham, M. R. Topp, and J. K. Blasie. 1983. Comparison of the kinetics of calcium transport in vesicular dispersions and oriented multilayers of sarcoplasmic reticulum membranes. *Biophys. J.* 44:365–373.

9. Blasie, J. K., L. Herbette, D. Pascolini, V. Skita, D. Pierce, and A. Scarpa. 1985. Time-resolved x-ray diffraction studies of the sarcoplasmic reticulum membrane during active transport. *Biophys. J.* 48:9–18.

10. Pascolini, D., L. G. Herbette, V. Skita, F. Asturias, A. Scarpa, and J. K. Blasie. 1988. Changes in the sarcoplasmic reticulum membrane profile induced by enzyme phosphorylation to $E_1 \sim P$ at ~16 Å resolution via time-resolved x-ray diffraction. *Biophys. J.* 54:679–688.

11. Ferandez-Belda, F., M. Kurzmack, and G. Inesi. 1984. A comparative study of calcium transients by isotopic tracer, metallochromic indicator and intrinsic fluorescence in sarcoplasmic reticulum ATPase. *J. Biol. Chem.* 259:9687–9698.

12. Asturias, F., and J. K. Blasie. 1989. Effect of $[Mg^{2+}]$ on the Ca^{2+} uptake kinetics and structure of the sarcoplasmic reticulum membrane. *Biophys. J.* 55:739–753.

13. Pascolini, D., and J. K. Blasie. 1988. Moderate resolution profile structure of the sarcoplasmic reticulum membrane under "low" temperature conditions for the transient trapping of $E_1 \sim P$. *Biophys. J.* 54:669–678.

14. Pachence, J. M., P. L. Dutton, and J. K. Blasie. 1981. The reaction center profile structure derived from neutron diffraction. *Biochim. Biophys. Acta Bioenergetics.* 635:267–283.

15. Herbette, L., A. Scarpa, J. K. Blasie, C. T. Wang, L. Hymel, J. Seelig, and S. Fleischer. 1983. The determination of the separate Ca^{2+} pump protein and phospholipid profile structures within reconstituted sarcoplasmic reticulum membranes via x-ray and neutron diffraction. *Biochim. Biophys. Acta.* 730:369–378.

16. Pascolini, D., J. K. Blasie, and S. M. Gruner. 1984. A 12 Å resolution x-ray diffraction study of the phase behavior and electron density profile of isolated bovine retinal rod outer segment disk membranes. *Biochim. Biophys. Acta Biomembranes.* 777:9–20.